The Crystal Complex of Phosphofructokinase-2 of *Escherichia coli* with Fructose-6-phosphate
KINETIC AND STRUCTURAL ANALYSIS OF THE ALLOSTERIC ATP INHIBITION*[S]

Ricardo Cabrera[‡1], **Mauricio Baez**[‡], **Humberto M. Pereira**[§], **Andrés Caniuguir**[‡], **Richard C. Garratt**[§], and **Jorge Babul**[‡]

From the ‡*Departamento de Biología, Facultad de Ciencias, Universidad de Chile, Santiago, Chile and the* §*Centro de Biotecnología Molecular Estrutural, Instituto de Física de São Carlos, Universidade de São Paulo, São Paulo, Brazil*

Substrate inhibition by ATP is a regulatory feature of the phosphofructokinases isoenzymes from *Escherichia coli* (Pfk-1 and Pfk-2). Under gluconeogenic conditions, the loss of this regulation in Pfk-2 causes substrate cycling of fructose-6-phosphate (fructose-6-P) and futile consumption of ATP delaying growth. In the present work, we have broached the mechanism of ATP-induced inhibition of Pfk-2 from both structural and kinetic perspectives. The crystal structure of Pfk-2 in complex with fructose-6-P is reported to a resolution of 2 Å. The comparison of this structure with the previously reported inhibited form of the enzyme suggests a negative interplay between fructose-6-P binding and allosteric binding of MgATP. Initial velocity experiments show a linear increase of the apparent $K_{0.5}$ for fructose-6-P and a decrease in the apparent k_{cat} as a function of MgATP concentration. These effects occur simultaneously with the induction of a sigmoidal kinetic behavior (n_H of approximately 2). Differences and resemblances in the patterns of fructose-6-P binding and the mechanism of inhibition are discussed for Pfk-1 and Pfk-2, as an example of evolutionary convergence, because these enzymes do not share a common ancestor.

In *Escherichia coli*, the glycolytic step of the ATP-dependent phosphorylation of fructose-6-P is catalyzed by two different phosphofructokinases, Pfk-1 and Pfk-2. Kinetic evidence indicates that these enzymes are subject to regulation by high concentrations of ATP (1, 2). It has been elegantly demonstrated for Pfk-2 that this regulation is important for avoiding a futile cycle of ATP hydrolysis under gluconeogenic conditions (3). Because Pfk-1 and Pfk-2 do not share a common ancestor, they pose an intriguing case of convergence in the evolution of kinases because not only do they recognize the same phosphoryl acceptor substrate, but also each has

independently evolved a mechanism for inhibition by the phosphoryl donor ATP.

Pfk-2 belongs to the ribokinase family of sugar kinases. Other phosphorylated sugars are recognized as substrates by members of the family such as tagatose-6-phosphate kinases and 1-phosphofructokinases, which form a monophyletic cluster with Pfk-2 (4). Within this group (the PfkB subfamily), inhibition of the enzymatic activity by MgATP has so far only been reported for Pfk-2. The kinetic mechanism of Pfk-2 has been characterized to consist of an ordered sequential addition of substrates where fructose-6-P binding to the active site is required for the catalytic binding of MgATP. However, it has been observed that, in the absence of fructose-6-P, MgATP is able to shift the state of aggregation of Pfk-2 from dimer to tetramer, leading to the proposal of an allosteric site for this nucleotide (2). Recently (5), our group reported the crystal structure of Pfk-2 in its tetrameric form bound to two ATP molecules and two Mg ions per monomer (the Pfk-2·(ATP)$_2$ complex). One ATP corresponds to the phosphoryl donor substrate of the reaction and shows a singular interaction with a second ATP, which, we conclude, must be acting as the enzyme inhibitor.

For Pfk-1, several mechanisms have been discussed in an attempt to explain the kinetics of substrate inhibition. Wang and Kemp (6) proposed that ATP inhibition results from substrate antagonism coupled with a steady-state random mechanism wherein the high rate of catalysis does not permit equilibration of the binding of the substrates. Berger and Evans (7, 8) proposed a model based on the displacement of a pre-existing R-T equilibrium by means of the presence of an allosteric site for MgATP. According to this model fructose-6-P[2] binds preferentially to the relaxed state "R," which predominates in the absence of MgATP. Large concentrations of MgATP shift the population toward the T state, which presents a very low affinity for fructose-6-P. Both mechanisms have been challenged by Reinhart's group using the principle of allosteric linkage (9, 10). According to their proposal, MgATP inhibition is originated by the allosteric communication between the active sites of the homotetrameric enzyme. Substrate binding antagonism is manifested when MgATP in the active site of one subunit acts to lower the affinity for fructose-6-P in the active site of another subunit (11). Fenton and Reinhart (12) demonstrated through the use of hybrid oligomers that a

[S] The on-line version of this article (available at http://www.jbc.org) contains supplemental text, equations, and Table S1.

The atomic coordinates and structure factors (code 3N1C) have been deposited in the Protein Data Bank, Research Collaboratory for Structural Bioinformatics, Rutgers University, New Brunswick, NJ (http://www.rcsb.org/).

[1] To whom correspondence should be addressed: Departamento de Biología, Facultad de Ciencias, Universidad de Chile, Casilla 653, Santiago, Chile. E-mail: ricabrer@uchile.cl.

[2] The abbreviation used is: fructose-6-P or F6P, fructose-6-phosphate.

tetramer of Pfk-1 with only one functional active site is unable to show substrate inhibition, highlighting the importance of intersubunit interactions for the regulatory mechanism of the enzyme. The crystal structure of Pfk-1 from *E. coli* in complex with its products, fructose-1,6-bisphosphate and MgADP, was solved by Shirakihara and Evans (13). Each subunit contributes with complementary parts of two active sites and two allosteric sites, being the complete tetramer required to form all eight sites. The allosteric site in Pfk-1 is not involved in the MgATP inhibition but rather binds other effectors such as ADP and GDP as activators and P-enolpyruvate as an inhibitor. At the active site, the fructose-1,6-bisphosphate molecule is bound mainly by polar groups, and its 6-phosphoryl group is held by two arginine residues that belong to a neighboring subunit.

In the case of Pfk-2, inhibition occurs at low concentrations of fructose-6-P and high concentrations of MgATP (2, 14). Although the increment of the fructose-6-P concentration decreases the inhibitory effect of MgATP, no kinetic mechanism has been proposed to model this phenomenon. A mutant Pfk-2 in which Tyr-23 has been replaced by Asp at the allosteric site ablates a crucial interaction with the adenine moiety of the inhibitor ATP, leading to a highly decreased inhibitory effect (5, 14).

In the present work we determined the crystal structure of Pfk-2 with fructose-6-P bound at the active site (the Pfk-2·F6P complex) to 2 Å resolution. We compared this structure with the Pfk-2·(ATP)$_2$ complex searching for insights into the conformational changes that originate substrate inhibition. Furthermore, a kinetic characterization of the ATP-induced inhibition is presented. The initial velocities, as a function of the concentration of fructose-6-P and MgATP (within noninhibitory and inhibitory ranges), were adjusted to different conceivable mechanisms by means of global fitting. A complex behavior was observed that may involve intersubunit active site communication. The features of fructose-6-P binding are discussed in comparison with Pfk-1 and sugar-phosphate kinases from the PfkB subfamily.

EXPERIMENTAL PROCEDURES

Crystallization and Data Collection—The enzyme was purified according to the method described by Parducci *et al.* (15). Crystals were grown by the vapor diffusion method in a hanging drop consisting of 2 μl of the protein stock solution (2 mg/ml of protein in 25 mM Tris-HCl pH 7.6 buffer, 10 mM MgCl$_2$, 30 mM DTT, and 6 mM fructose-6-P) and 2 μl of a reservoir solution comprising 23% PEG 4000, 100 mM sodium acetate, pH 4.75, and 200 mM ammonium acetate. Crystals appeared after 3 days at 18 °C.

X-ray diffraction data were collected at 100 K. Measurements were made on the MX2-LNLS beamline (λ = 1.43Å) using a Marmosaic 225 CCD detector, over 1° increments in φ for a total rotation of 120° up to 2.0 Å resolution. The data were indexed and integrated using the program MOSFLM (16) and scaled using the program SCALA from the CCP4 suite (17).

Structure Solution and Refinement—The structure of *E. coli* Pfk-2 in complex with fructose-6-phosphate was solved by

TABLE 1

Data collection parameters and structure refinement statistics

The values in parentheses are for the outer resolution shells.

Full data collection and refinement statistics	Pfk-2-F6P complex
Space group	C222$_1$
Cell dimensions (Å)	
a	68.72
b	153.78
c	223.80
Detector	Marmosaic 225
X-ray source	LNLS MX2
Wavelength (Å)	1.43
Resolution range (Å)	55.99–2.00 (2.11–2.00)
Redundancy	4.8 (4.4)
R_{meas} (%)	10.8 (57.6)
R_{sym} (%)	9.6 (50.8)
Completeness (%)	99.2 (99.2)
Total reflections	379253
Unique reflections	79638
$I/\sigma I$	12.6 (2.6)
Refinement parameters	
R (%)	18.19
R_{free} (%)	22.06
Ramachandran plot	
Most favored region (%)	94.0
Number of residues in disallowed regions	4
Overall B-factor (Å^2)	25.46
Ligand B-factor (Å^2)	22.52
Number of protein atoms	9039
Number of water molecules	1036
Number of ligand atoms	84
Root mean square bond lengths (Å)	0.01
Root mean square bond angles (Å)	1.29

molecular replacement using the Phaser program (18) and a monomer of the previously solved Pfk-2 structure in complex with ATP as a search model (Protein Data Bank code 3CQD). Model refinement was carried out with Phenix (19) employing TLS parameters (that describe the rigid body motion of large groups of atom using Translation, Libration, and Screw-rotation displacements) in the final stages of refinement. Model building was performed with COOT (20), using σ_A-weighted $2F_o - F_c$ and $F_o - F_c$ electron density maps. A total of 1041 water molecules were included (Table 1) using both COOT and Phenix. The fructose-6-phosphate molecules were added using COOT.

In all cases, the behavior of R_{free} was used as the principal criterion for validating the refinement protocol, and the stereochemical quality of the model was evaluated with Procheck (21) and Molprobity (22). Full statistics for data collection and refinement are summarized in Table 1.

Enzyme Measurements—Phosphofructokinase activity was determined spectrophotometrically coupling the fructose-1,6-bisphosphate production to the oxidation of NADH, according to Babul (23) and modified to avoid the occurrence of lag phases in the time courses (24). Activity measurements were performed in 25 mM Tris, pH 8.2, using a constant excess of 5 mM MgCl$_2$ with respect to the total ATP concentration. This condition maintains the free magnesium close to 5 mM for each concentration of free MgATP used (25). All of the measurements were carried out in 96-well plates and read with a microplate reader (Biotek, Synergy 25) at room temperature (25 °C). Each experiment was repeated at least three times and averaged to determine the errors bars at one standard deviation.

Mechanism of the ATP Allosteric Inhibition of Pfk-2

Treatment of Kinetic Data—*Ad hoc* models of competitive or partial substrate inhibition were tested. Coherent with the observation of two molecules of MgATP in the Pfk-2 structure (5), these models involve the binding of a second molecule of MgATP to the enzyme. Kinetics equations for competitive (supplemental Equation S1) or partial (supplemental Equation S2) models were derived using the rapid equilibrium assumption described by Segel (26). These models were adjusted to initial velocity data obtained as a function of MgATP at several different concentrations of fructose-6-P by means of a global fit procedure using the nonlinear regression tool provided by SigmaPlot 10.0 (SYSTAT Software Inc.) or DynaFit (27). Discrimination between the two models was performed with the DynaFit software using the Akaike index (supplemental materials). The constants of both equations represent the equilibrium and kinetics steps shown in Fig. 4*A*.

RESULTS

Overall Structure of the Subunit and Oligomeric State—As previously reported (5), the overall fold of Pfk-2 consists of one major domain with a central β-sheet surrounded by α-helices and one minor domain consisting of a four-stranded β-sheet. The active site is located within at a large cleft of the major domain formed along the C-terminal edge of the central β-sheet and covered by one side of the minor domain β-sheet. In that location we observed an electron density that could be readily modeled as a fructose-6-P molecule. In the remaining description presented here, we will make use of the secondary structure nomenclature described previously (5) in which β-strands 1, 4, 5, and 8–13 comprise the sheet of the major domain, and β-strands 2, 3a, 3b, 6, and 7 comprise the sheet of the minor domain.

The final structure revealed the presence of four monomers in the asymmetric unit associated in a way that strongly resembles the tetramer observed in the Pfk-2·(ATP)$_2$ complex (Fig. 1). The monomers are related by a 222 symmetry (a dimer of dimers), and each monomer makes contact with two others. In one case, the interface is formed by the orthogonal packing of the four-stranded β-sheet of the minor domains of adjacent subunits (A and D or B and C, respectively; Fig. 1*a*) and presents the β-clasp arrangement described previously (5). A solvent-accessible surface area of 1,262.6 Å^2 is buried by this interface (calculated on the basis of the A and D chains), which is 160.8 Å^2 less than the β-clasp interface of the Pfk-2·(ATP)$_2$ complex. It is this interface that is expected to be preserved when Pfk-2 is observed in its dimeric state. The other interface is formed by the association of two dimers through the region near the C-terminal strand of the major domain of opposing subunits and forms the contact surface between the A and C subunits on the one hand and between the D and B subunits on the other (Fig. 1*a*). This interface covers 1,828.6 Å^2 of the solvent-accessible surface area, showing a decrease of ~330 Å^2 relative to its counterpart in the Pfk-2·(ATP)$_2$ complex. Contrary to the tetrameric Pfk-2·(ATP)$_2$ complex, the minor domains do not contribute to this second interface (Fig. 1*b*).

A tetrameric association for the Pfk-2·F6P complex was unexpected. In solution and in the presence of fructose-6-P,
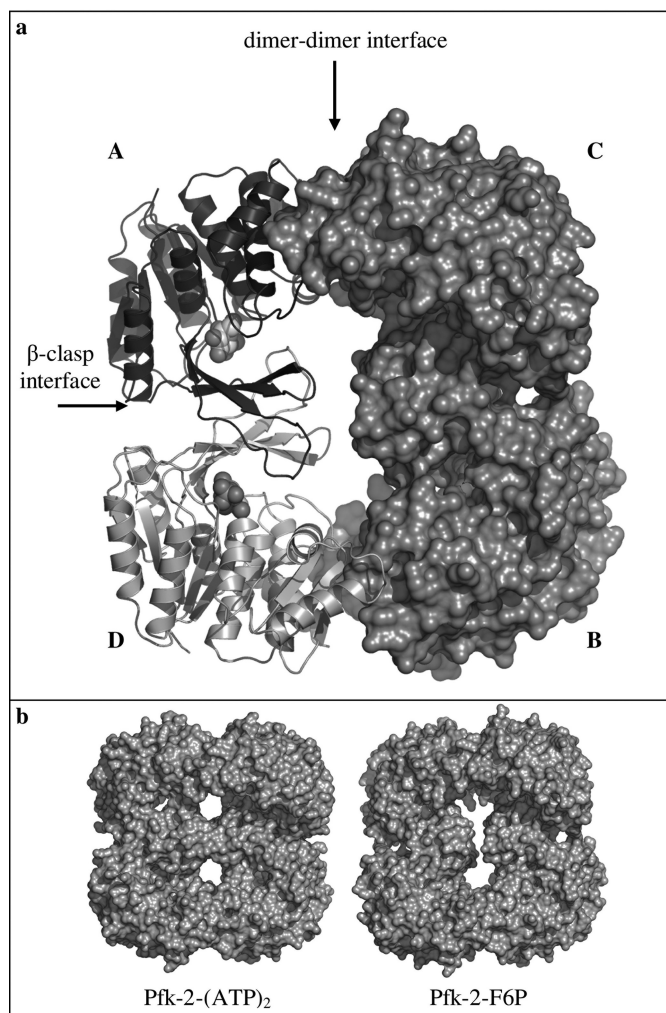
FIGURE 1. **Overall structure of the Pfk-2·F6P complex.** *Panel a*, the subunits A (*dark gray*) and D (*light gray*) are shown as ribbons, and the dimer BC is shown as a single surface. The fructose-6-P molecules are represented as space-filling models. *Panel b*, comparison of the tetrameric packing observed in the Pfk-2·(ATP)$_2$ and Pfk-2·F6P complexes. A major loss in the surface area of the dimer-dimer interface is accounted for by the absence of contacts between the minor domain barrels in the fructose-6-P-bound form.

Pfk-2 forms a dimer under previously studied conditions (2, 28). The tetramer we observe in the present study is therefore probably the result of energetically favorable crystal contacts. This presumably occurs because the dimer-dimer interface observed in the Pfk-2·(ATP)$_2$ complex remains largely available for establishing intermolecular contacts that are favored by the high protein concentrations reached during crystallization. In any case, as described above, an important reduction in the interfacial surface area is observed with respect to the Pfk-2·(ATP)$_2$ complex, which is known to be tetrameric in solution at every protein concentration tested (see references in Ref. 24). In the dimeric form of the enzyme, only the β-clasp interface would be expected to exist. This can be assumed on the basis of the fact that the integrity of this interface is essential for fructose-6-P binding and therefore catalysis, as described in the following section.

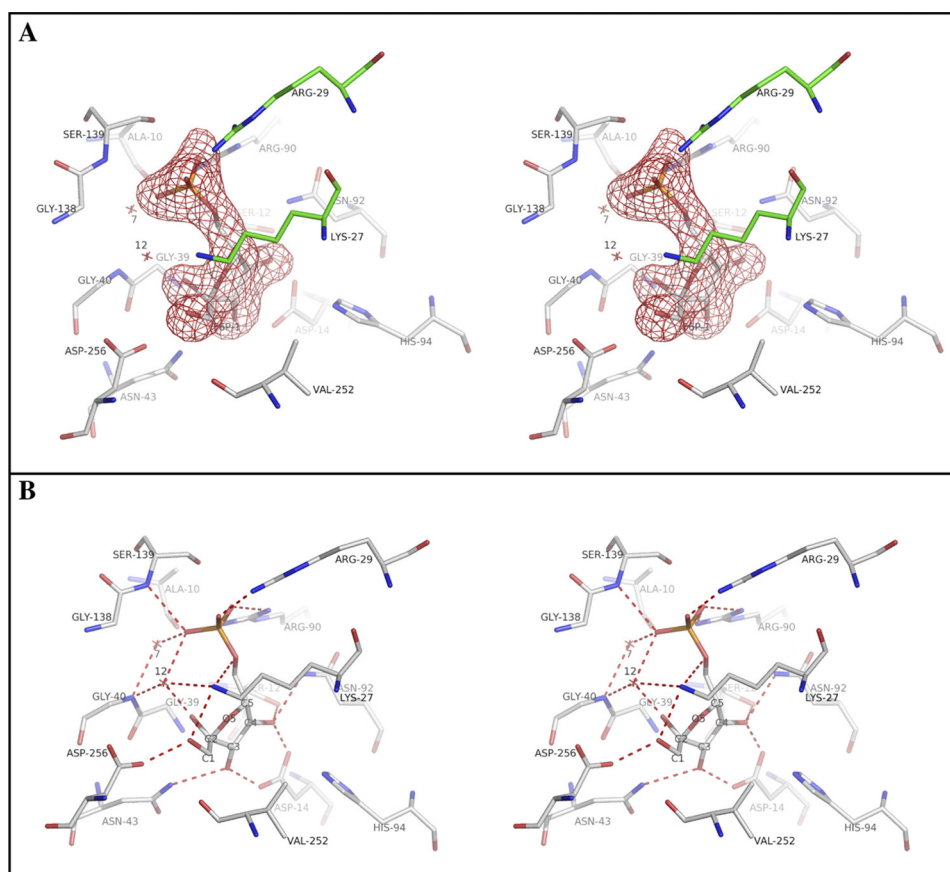*Fructose-6-P Binding*—The difference electron density map shows clearly the presence of a fructose-6-P molecule (Fig.

FIGURE 2. **The fructose-6-P-binding site of Pfk-2.** Stereo figure of the active site in chain D. *A*, electron density omit map ($F_o - F_c$) contoured at 3 σ for fructose-6-P is shown in *red*. Residues Lys-27 and Arg-29 come from subunit A and are highlighted in *green*. The locations of structural waters 7 and 12 are indicated by *red crosses*. *B*, a similar orientation of the active site highlighting the interactions described in the text. This figure was prepared using PyMOL.

2*A*) in each subunit. Interactions with this ligand are established by residues coming from both domains and from the adjacent subunit via the β-clasp interface.

The sugar molecule is observed in the β-D-fructofuranose form, adopting a puckering in which the out-of-plane atom, C2, is on the same side of the ring (*endo*) as C6. Although hydroxyl groups 3 and 4 are oriented toward opposite sides of the plane, they tend to an almost equatorial configuration, showing a torsion angle of $-33.2°$ along the C3–C4 bond (calculated on the basis of the ligand from the D subunit) and allowing for simultaneous interaction of both hydroxyls with the side chain of Asp-14. All of the hydroxyls groups and the phosphate moiety of the fructose-6-P ligand are involved in a network of direct and water-mediated hydrogen-bonds with protein residues (Fig. 2*B*). The OH1 group of the substrate forms a hydrogen bond with $O_{\delta1}$ of the Asp-256 side chain from $\alpha8$ and N_ζ from Lys-27 in $\beta3$ from the adjacent subunit of the dimer. OH2 is at a distance of 2.53 Å from water 12, which in turn interacts with the amide nitrogen from Gly-40 and O2P from the phosphate group of the sugar. Water 12 also lies spatially close to N_ζ of Lys-27 at a mean distance of 3.26 Å but presents poor hydrogen bonding geometry. OH3 directly contacts $N_{\delta2}$ of the Asn-43 side chain, the amide nitrogen from Gly-39, and $O_{\delta2}$ of the carboxylate side chain of Asp-14. $O_{\delta1}$ of Asp-14 interacts with OH4, which is in turn hydrogen-bonded to O_γ from Ser-12 and $N_{\delta2}$ of Asn-92. The

phosphate group establishes interactions with the guanidinium group of Arg-90 from the N-terminal end of $\beta6$ as well as Arg-29 and Lys-27 from $\beta3a$ of the adjacent subunit. Together with water 12, a second water molecule (number 7) bridges O2P to the amide group of Gly-40. Also, direct hydrogen bonds are established by both the O_γ and the amide group of Ser-139 with the phosphate moiety (Fig. 2*B*). The overall structure of the binding site and particularly the contributions made by neighboring subunits explain the requirement for an intact dimer to sustain substrate binding.

Structural superposition of the four monomers reveals differences in the relative orientation of their major and minor domains, suggesting that they present a degree of relative flexibility (supplemental materials). However, no significant differences are observed between the active site residues of the four chains in regard to the interactions made with fructose-6-P, except for the side chains of Arg-105 and His-94, which only in subunit D are within 4 Å of the sugar phosphate and some variation in the water structure.

Structural Differences between the Pfk-2·F6P and Pfk-2-(ATP)$_2$ Complexes at the Active Site—Conformational changes at the active site of Pfk-2 were evaluated by structural superposition of the Pfk-2·F6P and Pfk-2·(ATP)$_2$ complexes (Fig. 3). Most of the residues involved in interactions with the ADP moiety of the substrate ATP molecule show a similar conformation in the two complexes. The main difference cor-
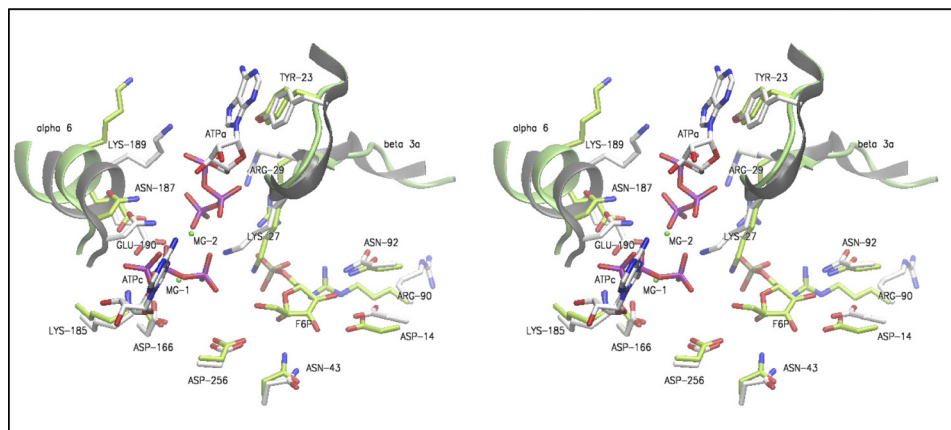
FIGURE 3. **Conformational changes at the active site of Pfk-2.** Stereo view of the superposition of the Pfk-2·F6P (chain D) and Pfk-2·(ATP)$_2$ structures. The substrate ATP (ATPc), allosteric ATP (*ATPa*; adenine-Tyr-23 π-stacking conformation), and F6P molecules are shown surrounded by several residues providing them with important interactions in their respective structures. Color is according to the Corey-Pauling-Koltun scheme except for carbon atoms in the Pfk-2·F6P complex, which are shown in *green*. Part of the secondary structural elements α6 and β3a (neighboring subunit) of the Pfk-2·F6P (*lime*) and Pfk-2·(ATP)$_2$ (*gray*) complexes are shown.

responds to a major displacement of helix α6 whose N terminus is involved in substrate ATP binding (Fig. 3). This region contains the N*XX*E motif (15, 29) where the residues Asn-187 and Glu-190 provide interactions with the β-phosphate of the substrate ATP and waters in the coordination sphere of Mg-1 in the Pfk-2·(ATP)$_2$ complex (5). In the Pfk-2·F6P structure, there was no electron density that could be modeled as a Mg^{2+} ion at the active site despite the latter being present in the crystallization conditions.

Four residues involved in direct contacts with the allosteric ATP show different positions in the Pfk-2·F6P complex (Fig. 3). The side chain of Lys-189 from helix α6 departs from the position observed in the Pfk-2·(ATP)$_2$ complex where it contacts the α-phosphate of the allosteric ATP. Asn-187 is also shifted further away from what would be the position of the γ-phosphate of the allosteric ATP, and waters that would form part of the coordination sphere of the second magnesium ion (Mg-2), which holds in place the γ-phosphate of the allosteric ATP, are lost. Furthermore, from strand β3a of the partner subunit, Tyr-23 is displaced from the position where it makes a π-stacking interaction with the adenine ring, and Lys-27, whose N$_\zeta$ lies between the γ-phosphates of the two ATP molecules in the Pfk-2·(ATP)$_2$ complex is recruited to form part of the hydrogen bonding network of fructose-6-P. Most of these shifts appear to be largely rigid body dislocations caused by alteration of the relative orientation of the subunits of the functional dimer and relative dislocations of individual elements of secondary structure, as appears to be the case with α6, for example.

At the fructose-6-P-binding site, the residues involved in the interaction with hydroxyl groups 1–4 show a similar conformation in the Pfk-2·(ATP)$_2$ complex (Fig. 3). However, conspicuous differences are seen for Lys-27, Arg-29, and Arg-90, residues mainly involved in interactions with the phosphate moiety of the sugar phosphate. In the case of Lys-27, N$_\zeta$ becomes displaced 3.27 Å away from its location near the γ-phosphates of the allosteric and substrate ATPs toward O1, O5, and the phosphate moiety of fructose-6-P. Furthermore, the side chains of Arg-29 and Arg-90 also become orientated

toward the substrate phosphate, forming direct hydrogen bonds. In the Pfk-2·(ATP)$_2$ complex, Arg-90 is orientated away from the active site, making a π-cation interaction with Trp-88 (5) and an ion pair with Asp-87. This conformational change requires a rotation of the χ_1 dihedral angle from -64.38 to $70.2°$ and suggests that Arg-90 plays a key role in substrate recognition.

The structure of the Pfk-2·F6P complex shows that most of the residues at the active site are prepared for the binding of the catalytic ATP, en route toward the ternary complex. On the other hand, as described above, it also demonstrates conformational changes that may indicate a potential negative interplay between allosteric ATP and fructose-6-P binding. For this reason, initial velocity experiments were performed to gain further insights about the pattern of inhibition that is originated by the interaction of these ligands with the enzyme.

Kinetic Characterization of the MgATP-induced Inhibition— Prior kinetic characterization of Pfk-2 was performed under noninhibitory conditions using low concentrations of MgATP (30). To understand how the allosteric binding of ATP affects the kinetic performance of Pfk-2, we here extend this characterization to cover the range of MgATP concentrations where inhibition is observed. As a starting point, we take the general scheme shown in Fig. 4*A*, which includes the minimum number of intermediate species between the two structurally determined forms of Pfk-2. The free enzyme can bind fructose-6-P and form the Pfk-2·F6P complex or sequentially bind two ATP molecules and form Pfk-2·(ATP)$_2$. It seems obvious that the binding of the substrate ATP is required for the binding of the allosteric ATP, because the γ- and β-phosphates of the latter are coordinated by a magnesium ion complexed to the γ- and β-phosphates of the former (5). In this scheme, the catalytic ternary complex of Pfk-2 (with rate constant k_{cat1}) could be formed from either Pfk-2·F6P or the intermediate specie Pfk-2-ATP, implicitly indicating a random mechanism. Additionally, this model allows the formation of a quaternary complex Pfk-2·F6P-(ATP)$_2$, generated by fructose-6-P binding

A

B
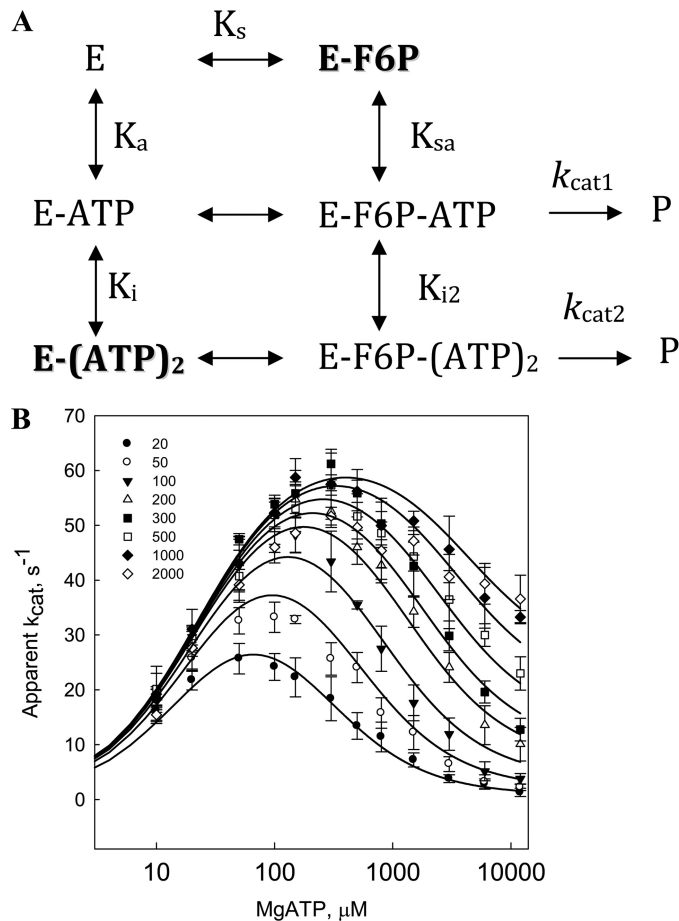
FIGURE 4. **Inhibition of Pfk-2 by MgATP.** *A*, general kinetic model for MgATP-induced inhibition. *E* represents Pfk-2. The full model correspond to a partial mechanism of substrate inhibition that, in the absence of the formation of the Pfk-2·F6P-$(ATP)_2$ complex, stands for a pure competitive mechanism of substrate inhibition. *B*, initial velocities of Pfk-2 as a function of MgATP concentration at different fixed fructose-6-P micromolar concentrations (as indicated by the *symbols*). The *continuous lines* describe the expected variation of the initial velocity obtained by a global fit of the partial substrate inhibition model to the experimental data. The values obtained for the constants are indicated in Table 2.

to Pfk-2·$(ATP)_2$ or ATP binding to the Pfk-2·F6P-ATP complex, that may be catalytically competent (k_{cat2}).

When MgATP was varied at several fixed concentrations of fructose-6-P (Fig. 4*B*), a bell-shaped dependence of the initial rate is observed. The increment of the fructose-6-P concentration attenuates the inhibitory portion of the curve and shifts the peak of maximum velocity toward higher concentrations of ATP. This behavior is not compatible with an uncompetitive mechanism of substrate inhibition based on the formation of an abortive complex between the inhibitory substrate and the reaction product (31). Therefore, a negative interplay between fructose-6-P and MgATP in the forward side of the reaction was considered a better scheme to propose models. Global fit analysis of this data to models describing complete and partial substrate inhibition was performed.

The mechanism of pure competitive inhibition based in the formation of an abortive complex, E-ATP$_2$, poorly fit the data (not shown) because inhibition by MgATP still occurs at high concentrations of fructose-6-P, and it seems to attain a plateau of nonzero activity, which is not predicted by that model.

TABLE 2

Parameters obtained for a model of partial inhibition

The meanings of constants are according to Fig. 5*A*. The values of k_{cat} have units of s^{-1}. Dissociation constants are given in μM.

Constants	Values ± error
K_s	6 ± 5
K_a	13 ± 12
K_{sa}	22 ± 1
K_i	81 ± 26
K_{i2}	5758 ± 1395
k_{cat1}	65 ± 1.2
k_{cat2}	34 ± 3.3

A better fit was obtained with a model of partial substrate inhibition under rapid equilibrium operating in the context of a random mechanism of substrate addition to the active site (Fig. 4*B*). Statistical discrimination analyses between these models and a model that considers the Pfk-2·F6P-$(ATP)_2$ complex to be inactive also support the partial mechanism of substrate inhibition. A model of partial inhibition predicts that the structure of Pfk-2 is able to accommodate the allosteric ATP in a configuration, which is still compatible with catalysis by the enzyme, suggesting that in addition to the inactive Pfk-2·$(ATP)_2$ complex, a partially active species, Pfk-2·F6P-ATP$_2$, is formed. The kinetic constants derived from adjusting this model are shown in Table 2. According to this result, fructose-6-P could bind the Pfk-2·$(ATP)_2$ complex with a constant of 746 μM compared with 6 μM for the free enzyme.

Initial velocities were analyzed as a function of fructose-6-P at several concentrations of MgATP (Fig. 5). From these curves, secondary plots were obtained to follow the effect of MgATP on k_{cat}, K_m, and the Hill coefficient. A complex behavior was observed in which the effect of MgATP can be split into two regions of nucleotide concentration. On the one hand, up to 100 μM of MgATP, k_{cat} for fructose-6-P increases to reach a maximum value of 60 ± 4 s^{-1} (Figs. 5*A* and 6*A*). This increment is consistent with the saturation of the catalytic site with MgATP because the apparent K_m for MgATP was ~22 μM (Table 2). Within the same interval, the saturation curves of fructose-6-P are hyperbolic (Fig. 5*A*) with a half-saturation point ($K_{0.5}$) that increases (from 4.5 to 30 μM) with the concentration of MgATP (Fig. 6*B*). On the other hand, at concentrations over 0.5 mM MgATP, the k_{cat} value decreases from 60 ± 4 s^{-1} to a final value of 44 ± 1 s^{-1} (Fig. 6*A*), whereas $K_{0.5}$ keeps raising linearly with the MgATP concentration, without signs of an apparent saturation (Fig. 6*B*). Within this interval, saturation curves for fructose-6-P change from hyperbolic to sigmoid until they reach a Hill value of 2 above 1.5 mM of MgATP (Fig. 6*C*). Although the linear variation of the half-point of saturation for fructose-6-P is reminiscent of a pure competitive mode of inhibition, this mechanism is not compatible with the decrease of k_{cat} to a finite value and the sigmoidal saturation induced at elevated concentrations of MgATP.

DISCUSSION

MgATP-induced Inhibition: Competitive or Partial?—The comparison of the Pfk-2·F6P complex with the previously reported Pfk-2·$(ATP)_2$ form shows conformational changes that
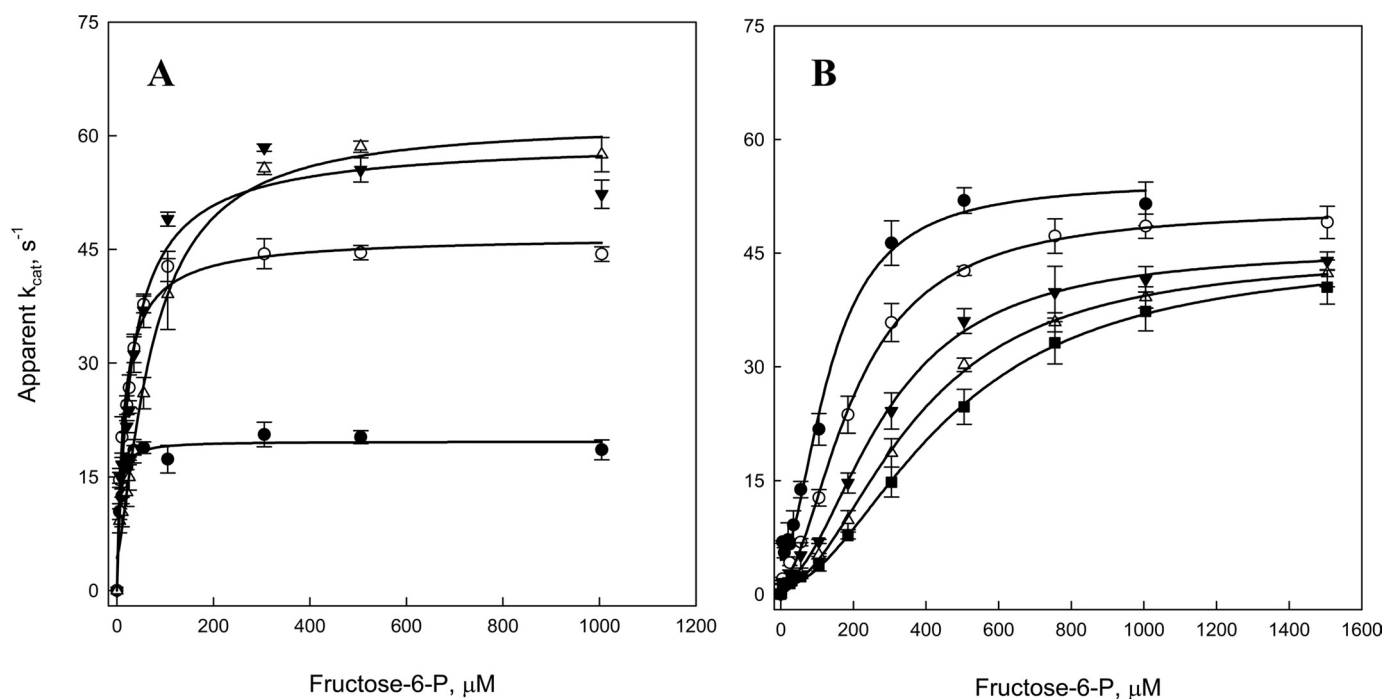
FIGURE 5. **Kinetics for fructose-6-P at different concentrations of MgATP.** Initial velocities of Pfk-2 were obtained with fructose-6-P as variable substrate at different fixed concentrations of MgATP from 10 μM to 10 mM. Kinetics measured with 10 (●), 50 (○), 500 (▼), and 800 μM (△) of MgATP are shown in *A*. Kinetics measured with 1500 (●), 3000 (○), 5000 (▼), and 10000 μM (△) of MgATP are shown in *B*. The *continuous lines* represent the individual fit of each curve to the Hill equation.
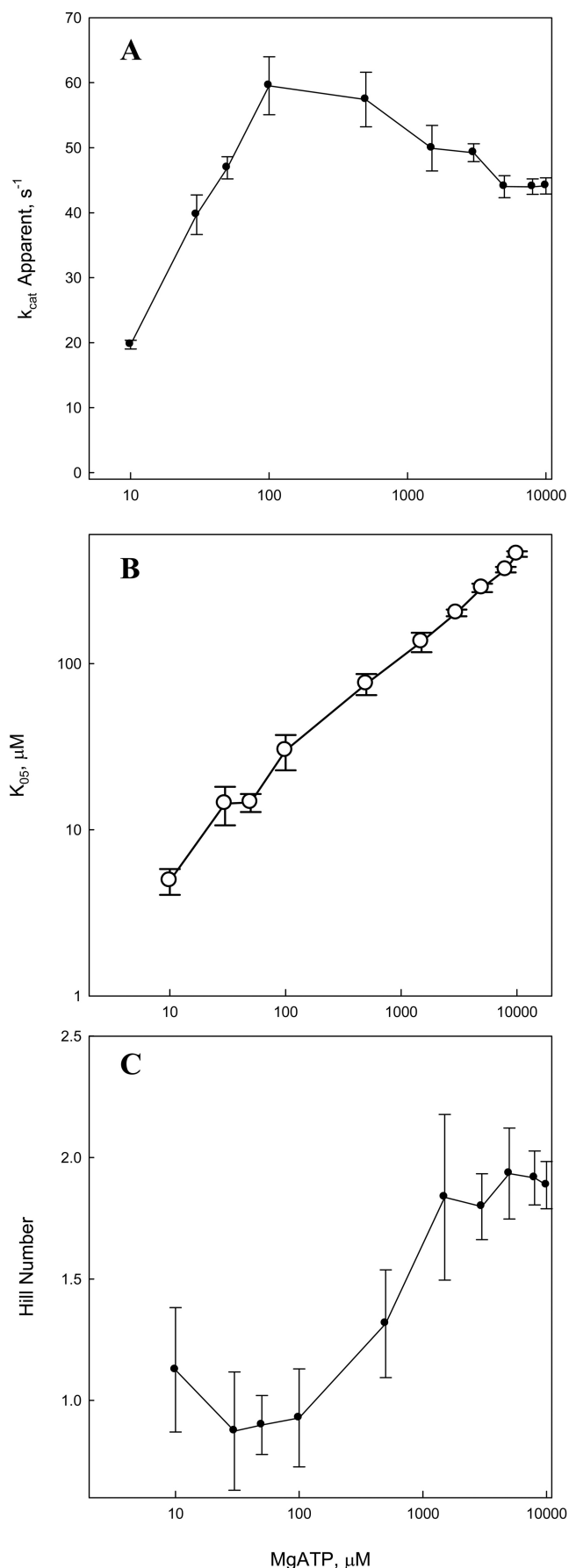
indicate a mutual negative interplay between the binding of allosteric ATP and fructose-6-P. Two possible outcomes are expected: a quaternary complex Pfk-2·F6P-(ATP)$_2$ could be formed or not.

If the Pfk-2·(ATP)$_2$ configuration were unable to bind the sugar phosphate substrate, a mechanism of pure competitive inhibition would be envisioned. In this case, the Pfk-2·(ATP)$_2$ complex corresponds to the dead-end species, and the productive binding of fructose-6-P is represented by the Pfk-2·F6P structure reported here. This would explain the linear increase of 100 times the half-saturation point for fructose-6-P induced by MgATP (Fig. 6*B*). However, this model poorly adjusts initial velocity curves for MgATP at different fixed concentrations of fructose-6-P (global fit not shown). Also, deviations are evident when analyzing the initial velocity curves for fructose-6-P at different fixed concentrations of MgATP, because either the sigmoidal behavior (Figs. 5*B* and 6*C*) or the dependence of k_{cat} with the MgATP concentration shown by Pfk-2 (Fig. 6*A*) is not compatible with a pure competitive inhibition mechanism.

In the case of Pfk-1, MgATP inhibition has been described as partial inhibition. MgATP inhibits the enzyme by a K-type mechanism decreasing its apparent affinity for fructose-6-P with little or no effect on k_{cat} (11). More importantly, the increment of K_{05} for fructose-6-P reaches a plateau at ~3 mM MgATP. This has been considered as evidence that Pfk-1 can simultaneously support catalytic turnover and binding of inhibitory ATP. In this framework, the application of linkage function analysis shows that ATP inhibition arises by a positive free energy of coupling because of the negative mutual influence between the ATP and fructose-6-P-binding sites

(11). Likewise for Pfk-2, if the Pfk-2·(ATP)$_2$ complex structure were able to bind the sugar phosphate and perform catalysis, a mechanism of partial inhibition would be in operation. The decrease of k_{cat} to reach a finite value (Fig. 6*A*) is suggestive of the formation of a partially active Pfk-2·(ATP)$_2$·F6P complex, but in opposition to Pfk-1, we do not detect a plateau for the variation of K_{05} for fructose-6-P even at 10 mM MgATP (Fig. 6*B*). In this case, the application of the linkage function analysis to Pfk-2 would result in a free energy of coupling with either an infinite value, when considering the competitive nature of K_{05} variation of fructose-6-P or a finite value when taking into account the variation of k_{cat} for fructose-6-P because of its partial nature (32). Hence, a more complex mechanism is needed to apply such thermodynamic formalism to the substrate inhibition of Pfk-2. At any rate, we could fairly say that MgATP appears to be acting not only as a K-type inhibitor (antagonizing the binding of fructose-6-P) but also as a V-type inhibitor (decreasing the value of k_{cat}).

It would be hard to explain every observed kinetic feature exclusively from our observations made by comparing the allosteric ATP-bound complex and the sugar-bound complex of Pfk-2. However, there are specific conformational changes that help to explain the decrease of the apparent affinity for fructose-6-P induced by MgATP. With respect to the interactions observed in the fructose-6-P complex, binding of the allosteric ATP seems to perturb the network of interactions with the phosphate moiety, mainly sequestering the side chain of Lys-27 and reorienting the side chain of Arg-90 out the active site (Fig. 3). Because allosteric ATP and Arg-90 are far apart in the active site, it is not obvious how the conformational change of this residue is caused by the allosteric bind-

ing of ATP. In the case of Lys-27, it forms interactions with both ATP γ-phosphates in the Pfk-2·(ATP)$_2$ complex, whereas it is central to the hydrogen bonding network which secures the sugar phosphate in the complex with fructose-6-P. Indeed, in two of the subunits, Lys-27 forms an additional water-mediated hydrogen bond to O3P of the phosphate group of fructose-6-P, reinforcing its central role in fructose-6-P binding. Because it is difficult to reconcile how Lys-27 could simultaneously perform these two roles, the ligand that comes first (either fructose-6-P or the allosteric ATP) to the active site would diminish the affinity for the second. However, the kinetic characterization of Pfk-2 still requires further studies to fully describe the complexity of the inhibition mechanism. The use of allosteric site mutants and the structure determination of ternary complexes with nonhydrolyzable ATP analogues might be helpful in this elucidation. In any case, none of these models anticipate the sigmoid behavior clearly shown by the saturation of fructose-6-P at high concentrations of MgATP, where a Hill coefficient of 2 is reached (Fig. 6C).

Sigmoidicity of Fructose-6-P Curves at Inhibitory Concentrations of MgATP—Although the homodimeric state of Pfk-2 is required for enzymatic activity and stability (33, 34) and is entirely consistent with the participation of both subunits in the formation of the active sites, no role for communication between these sites has been suggested previously. Sigmoid substrate binding induced by an allosteric inhibitor is a feature predicted by specific models of mechanisms that involve allosteric communication among binding sites in oligomeric proteins, such as Monod-Waymann-Changeaux (35) and Koshla and-Nemethy-Filmer (36), and general models of allosteric site interactions (10, 31, 37). These models have been used to explain the sigmoid saturation of fructose-6-P upon increasing the MgATP concentration in Pfk-1, but details about the conformational changes are unknown. Using hybrid tetramers of Pfk-1, Fenton and Reinhart (12) have dissected the allosteric interactions between the two substrates fructose-6-P and MgATP. They concluded that MgATP inhibition is independent of fructose-6-P cooperativity because a hybrid tetramer with only one site for fructose-6-P still shows ATP inhibition.

Different from Pfk-1, Pfk-2 presents an allosteric site in each subunit. Several contacts with either fructose-6-P or the allosteric ATP are formed by side chains from the β3a strand of the adjacent subunit of the dimer (Fig. 3). It is therefore conceivable that binding of the allosteric ATP could also promote changes in the communication between the active sites via the residues directly involved in its binding, leading to co-operativity. It is noteworthy that some structural differences at the β-clasp interface are related to changes in the shape of the active site. For example, the large conformational change of Arg-90, necessary for fructose-6-P binding, leads to an alteration of the Trp-88 side chain conformation directly in-

FIGURE 6. **Effect of MgATP on the apparent kinetic parameters for fructose-6-P.** A, k_{cat}. B, $K_{0.5}$. C, Hill coefficient. The values of each saturation curve were obtained from individually fitting the curve of Fig. 5 to the Hill equation and plotted against the concentration of MgATP.

volved in intersubunit contacts (5). The loss of the π-cation interaction of Trp-88 and Arg-90 is consistent with a significant increment in the intrinsic fluorescence emission of the enzyme in solution, when comparing the fructose-6-P- and MgATP-bound forms (38). In the Pfk-2·F6P complex, the surface area buried in the β-clasp interface is less than that in Pfk-2·(ATP)$_2$ complex. In addition, whereas the Pfk-2·F6P complex presents variable relative orientations of their minor domains (supplemental materials), the Pfk-2·(ATP)$_2$ complex is restricted to a fixed position. This is in agreement with previous observations from SAXS measurements of Pfk-2 in solution. In this case, different relative orientations of the major and minor domains of a homology model do not cause high discrepancies with the SAXS curves of the fructose-6-P-bound form of the enzyme, but it does with the curves in the presence of MgATP (39).

In this way, conformational changes at the sugar phosphate site and at the relative orientation of the major and minor domains, inferred from the comparison of both crystal complexes of Pfk-2, are consistent with the behavior in solution and help to explain the negative interplay observed by enzyme kinetics. Thus, we consider that the present structure captures most of the features associated with fructose-6-P binding in solution, despite the crystal contacts showing a tetrameric association that is not observed otherwise.

In addition to the β-clasp interface that originates the functional homodimer, the presence of MgATP generates the definitive dimer-dimer interface leading to homotetramer formation. Prior work from our group has shown that substrate inhibition induced by MgATP remains in mutant enzymes that are unable to form tetramers (24). Preliminary results demonstrate that these mutants also show the hyperbolic-sigmoid transition observed for the wild type, arguing against this phenomenon having its origin in tetramer formation.

Structural Determinants for Binding of Fructose-6-P in Different Scaffolds—The first reported phosphofructokinase x-ray structure was for a homologue of Pfk-1, the phosphofructokinase from *Geobacillus stearothermophilus* in complex with fructose-6-P and ADP (40). In 1988, Shirakihara and Evans (13) presented the crystal structure of Pfk-1 from *E. coli* complexed to its products fructose-1,6-bisphosphate and ADP. Similar to Pfk-2, the hydroxyl groups of the sugar ligand in Pfk-1 participate in a network of hydrogen bonds, but in this case a nonpolar interaction (with Met-169) is also observed. The most striking feature is that two positively charged residues from a neighboring subunit (Arg-162 and Arg-243) contribute to the binding of the 6-phosphate moiety in an analogous fashion to that observed for Lys-27 and Arg-29 in Pfk-2, suggesting that intact quaternary interactions are essential for catalysis in both cases.

Slight differences are observed between the structure of fructose-6-P in Pfk-1 and Pfk-2. For example, hydroxyls 3 and 4 appear to approach a more planar configuration with respect to the furanose ring. Dihedral O3-C3-C4-O4 of fructose-6-P is -86.76 in Pfk-1 (Protein Data Bank code 1PFK chain A), compared with -33.23 observed in Pfk-2. The interaction of the Asp-14 carboxylate with both hydroxyls in Pfk-2 seems to be responsible for restraining this geometry, making

it more equatorial than in Pfk-1, where these hydroxyls are bound by different residues. With respect to catalysis, Asp-127 in Pfk-1 is believed to be the general base, which abstracts a proton from OH1, thereby facilitating nucleophilic attack on the γ phosphate of ATP. In Pfk-2, the analogous base is also an aspartic acid (Asp-256), which is hydrogen-bonded to OH1 in the structure described here and presumably operates by a similar general mechanism.

Prior to this report, from a total of 54 protein structures found in the Protein Data Bank containing a fructose-6-P ligand, only two correspond to phosphofructokinases (EC 2.7.1.11). Furthermore, within the PfkB subfamily, only Pfk-2 and the phosphotagatose kinases from *Staphylococcus aureus* (Protein Data Bank code 2jg1) and *Listeria innocua* (Protein Data Bank code 3jul) present three-dimensional structures with the phosphoryl-acceptor substrate bound, showing there to be a relative paucity of structural information concerning the recognition and discrimination of sugar phosphates within this major branch of the ribokinase family. Miallau *et al.* (41) described aspects of phosphosugar recognition in the structure of tagatose-6-phosphate kinase from *S. aureus*, identifying a conserved motif where a Ser residue, homologous to Ser-139 of Pfk-2, establishes a hydrogen bond with the phosphate of tagatose-6-phosphate. The identification of a similar interaction here would seem to bear out this proposal. On the other hand, the structural basis for discrimination presumably revolves around carbon 4, the only position to present inverted chirality in the two sugars. In Pfk-2, Asn-92 makes a hydrogen bond to hydroxyl 4 of fructose-6-P, whereas in phosphotagatose kinases, a Cys residue (Cys-90 in 2jg1 and Cys-92 in 3jul) replaces Asn at this position and presents a close contact between its thiol group and the C4 and O4 of tagatose-6-phosphate, suggesting a role in substrate discrimination. Together with the crystallographic studies of their respective complexes, a thorough sequence analysis of the PfkB subfamily is necessary to understand fully how sequence traits are related to selectivity toward their phosphosugar substrates.

REFERENCES

1. Atkinson, D. E., and Walton, G. M. (1965) *J. Biol. Chem.* **240,** 757–763
2. Kotlarz, D., and Buc, H. (1981) *Eur. J. Biochem.* **117,** 569–574
3. Torres, J. C., Guixé, V., and Babul, J. (1997) *Biochem. J.* **327,** 675–684
4. Cabrera, R., Babul, J., and Guixé, V. (2010) *Arch. Biochem. Biophys.* **502,** 22–30
5. Cabrera, R., Ambrosio, A. L., Garratt, R. C., Guixé, V., and Babul, J. (2008) *J. Mol. Biol.* **383,** 588–602
6. Wang, X., and Kemp, R. G. (2001) *Biochemistry* **40,** 3938–3942
7. Berger, S. A., and Evans, P. R. (1991) *Biochemistry* **30,** 8477–8480
8. Berger, S. A., and Evans, P. R. (1992) *Biochemistry* **31,** 9237–9242
9. Wyman, J. (1965) *J. Mol. Biol.* **11,** 631–644
10. Weber, G. (1972) *Biochemistry* **11,** 864–878
11. Johnson, J. L., and Reinhart, G. D. (1992) *Biochemistry* **31,** 11510–11518
12. Fenton, A. W., and Reinhart, G. D. (2003) *Biochemistry* **42,** 12676–12681
13. Shirakihara, Y., and Evans, P. R. (1988) *J. Mol. Biol.* **204,** 973–994

14. Guixé, V., and Babul, J. (1985) *J. Biol. Chem.* **260,** 11001–11005
15. Parducci, R. E., Cabrera, R., Baez, M., and Guixé, V. (2006) *Biochemistry* **45,** 9291–9299
16. Leslie, A. G. (2006) *Acta Cryst.* **D62,** 48–57
17. Collaborative Computational Project, Number 4. (1994) *Acta Cryst.* **D50,** 760–763
18. McCoy, A. J., Grosse-Kunstleve, R. W., Adams, P. D., Winn, M. D., Storoni, L. C., and Read, R. J. (2007) *J. Appl. Crystallogr.* **40,** 658–674
19. Adams, P. D., Grosse-Kunstleve, R. W., Hung, L. W., Ioerger, T. R., McCoy, A. J., Moriarty, N. W., Read, R. J., Sacchettini, J. C., Sauter, N. K., and Terwilliger, T. C. (2002) *Acta Cryst.* **D58,** 1948–1954
20. Emsley, P., and Cowtan, K. (2004) *Acta Cryst.* **D60,** 2126–2132
21. Laskowski, R. A., MacArthur, M. W., Moss, D. S., and Thornton, J. M. (1993) *J. Appl. Crystallogr.* **26,** 283–291
22. Davis, I. W., Murray, L. W., Richardson, J. S., and Richardson, D. C. (2004) *Nucl. Acids Res.* **3,** 615–619
23. Babul, J. (1978) *J. Biol. Chem.* **253,** 4350–4355
24. Baez, M., Merino, F., Astorga, G., and Babul, J. (2008) *FEBS Lett.* **582,** 1907–1912
25. Cornish-Bowden, A. (2004) *Fundamental of Enzyme Kinetics*, p. 88. Portland Press, London
26. Segel, I. H. (1975) *Enzyme Kinetics*, p. 22, Wiley, New York
27. Kuzmic, P. (1996) *Anal. Biochem.* **237,** 260–273
28. Guixé, V., and Babul, J. (1988) *Arch. Biochem. Biophys.* **264,** 519–524
29. Maj, M. C., Singh, B., and Gupta, R. S. (2002) *Biochemistry* **41,** 4059–4069
30. Campos, G., Guixé, V., and Babul, J. (1984) *J. Biol. Chem.* **259,** 6147–6152
31. MacRae, I. J., and Segel, I. H. (1999) *Arch. Biochem. Biophys.* **361,** 277–282
32. Reinhart, G. D. (2004) *Methods Enzymol.* **380,** 187–203
33. Baez, M., Cabrera, R., Guixé, V., and Babul, J. (2007) *Biochemistry* **46,** 6141–6148
34. Baez, M., and Babul, J. (2009) *FEBS Lett.* **583,** 2054–2060
35. Monod, J., Wyman, J., and Changeux, J. P. (1965) *J. Mol. Biol.* **12,** 88–118
36. Koshland, D. E., Jr., Némethy, G., and Filmer, D. (1966) *Biochemistry* **5,** 365–385
37. Weber, G. (1992) *Protein Interactions*, pp. 31–55, Chapman and Hall, New York
38. Guixé, V., Rodríguez, P. H., and Babul, J. (1998) *Biochemistry* **37,** 13269–13275
39. Cabrera, R., Fischer, H., Trapani, S., Craievich, A. F., Garratt, R. C., Guixé, V., and Babul, J. (2003) *J. Biol. Chem.* **278,** 12913–12919
40. Evans, P. R., and Hudson, P. J. (1979) *Nature* **279,** 500–504
41. Miallau, L., Hunter, W. N., McSweeney, S. M., and Leonard, G. A. (2007) *J. Biol. Chem.* **282,** 19948–19957